International Journal of Civil Engineering, Construction and Estate Management
Vol.6, No.4, pp.1-30, December 2018
Published by European Centre for Research Training and Development UK (www.eajournals.org)

STUDY ON LIMIT STATE OF EMBEDDED PERFOBOND RIB SHEAR CONNECTORS

MOHAMMED ANAGMI[1], AL-OTHMANI ABDULWASEA[2], KHALIL AL-BUKHAITI[3,*]

[1 3] School of Civil Engineering, south west Jiaotong University, Chengdu, Sichuan, China.
[2] School of Mechanical Engineering, south west Jiaotong University, Chengdu, Sichuan, China.

ABSTRACT: *As a major component of the joint zone steel-concrete composite bridge, the perfobond rib shear connectors (in German, or perfobond leiste, or in short, PBL) are widely used in recent years. Studies on PBL are relatively complete, while some results show a difference in significant between composite PBL and embedded PBL. Therefore, the limiting state and ultimate bearing capacity of the embedded PBL are examined in the current work based on some experimental studies and analysis of finite elements, on the following aspects: (1) FEA (finite element analysis) may suffer from poor convergence and low computational efficiency, while the simplified model cannot reflect local stress. Based on the test system of anchorage of Yangtze River Bridge 4 in Nanjing, the design parameters and embedded PBL dimensions were described; the relevant test results were summarized and analyzed. (2) Some detailed FEA models have been built according to the experience of the Yangtze 4 Yangtze River Bridge Anchorage System in Nanjing. Standard static analysis, extend the finite element method (XFEM), virtual crack closure technique (VCCT) are applied, is most suitable for this situation. (3) Six models of FEA models are constructed through one variable method to investigate the influencing factors on the ultimate bearing status of the embedded PBL. The results of these models are shown: the reinforcement ratio cannot affect the mechanical properties of the embedded when the ratio is 4 times lower than the diameter of the hole in concrete in a steel slab area. Through dimensional analysis, parameters that affect the mechanical properties of the embedded PBL can be rearranged in two dimensionless fitting a power function of the ability to represent the load-slip relationship of the embedded PBL shear connectors.*

KEYWORDS: Embedded PBL, Perfobond Rib Shear, Load Slip, Composite PBL, ABAQUS, FEM, Structure Bridge

---

INTRODUCTION

The recent period of construction has witnessed a great development observed through modern technologies that have been launched recently. In another hand, the studies and engineering designs have moved from the stage of the study of the forces exerted on the establishment to the emergence of new changes according to the requirements of modern technology. This technique has made the distribution of forces and stresses vary according to the type and shape of the profile used. According to the transition to modern construction based on the large span and the transfer of loads in a safe and varied manner without any side effects, In our research, we have studied many scientific papers and thesis that are discussed in this field and are based on several dissertation, which revolve around several different aspects, namely the strength of the form of the perfobond, as well as the number of holes in it, and the transverse rebar and plate connected to it. And the invitations in research results according to modern technology of engineering construction and modern construction.

ISSN 2055-6578(Print), ISSN 2055-6586(online)

Due to the current specification, the diameter of the perforated steel plate of the embedded PBL shear connector, the thickness of the perforated steel plate, the diameter of the transverse rebar, the strength of the concrete, the size of the outer concrete block, and the arrangement of the ordinary steel bars are not clearly defined, so different Test results obtained from test sizes and parameters will also vary. When designing the test, most of them are designed according to the actual structural size, in view of the current research on the embedded PBL shear connector, the main research contents of this paper are as follows:

1) the experimental data of embedded PBL shear connectors are sorted out and studied: based on the test of Nanjing Yangtze River Fourth Bridge main cable cross-fixing system, the design parameters and test results of part of the test specimens and based on the test results, the sign that embedded PBL shear connectors reach the limit state is put forward.

2) Finite element simulation study of embedded PBL shear connector: the connector of finite element analysis of embedded PBL shear connector is to simulate the fracture and failure of the concrete block, so it is necessary to have a suitable concrete constitutive model. Based on the Sidoroff Energy equivalence principle and the stress and strain relationship in Gb50010-2010 concrete structure design code, the value formula of concrete damage variable is deduced, and its reliability and superiority are verified by comparing it with several commonly used value formulas at present

Experimental Work

In order to grasp the mechanical behavior of the embedded PBL shear connector, it should be designed according to the actual original structure, but because of its very large system structure, the test equipment loading test can be limited, and the test cost is limited. The actual structure is different from the structural form of the standard launch test.

The entire test was divided into three trials, the first test was the type selection test, and 16 specimens were designed for loading test. In the second test, two PBL shear connectors with different parameters were screened out in the first test, and 11 specimens were designed. The third experiment is to study the shear bond performance of the final selected size. For ease of identification, the test pieces of the three tests are now renumbered as follows (note that the number is only applicable to the test piece in the test and does not apply to the finite element model of different parameters. Now we can explain terms for a specimen like:

(1) Specimen number "Axx-yy-zd" or "A" in "Axx-yy-zs" means a type A specimen, i.e., shear bond under the condition of pull-shear compound stress.

(2) "XX" means the diameter of the steel plate opening, and "yy" means the diameter of the steel bar passing through the heaven bar, all in millimeters.

(3) "Z" takes 1, 2 or 3, representing the first, second or third test.

(4) "D" means two shear bonds in a specimen, and "S" means only one shear bond in a specimen.

In the first experiment, a 1:1 model of two shear bonds was used; in the second experiment, in addition to a 1:1 model of two shear bonds, there was a single shear. The 1:1 model of the connector; the test piece in the third test is all a 1:1 model of a single shear bond. The size ratio of the test piece is chosen to be 1:1 to eliminate the effect of the scale effect**.** At a ratio of 1:1, the test piece consists of four parts: the base, the concrete block of the shear connector zone,

ISSN 2055-6578(Print), ISSN 2055-6586(online)

the shear connector, and the steel plate. The specific structure is shown from Figure 1 to Figure 5.

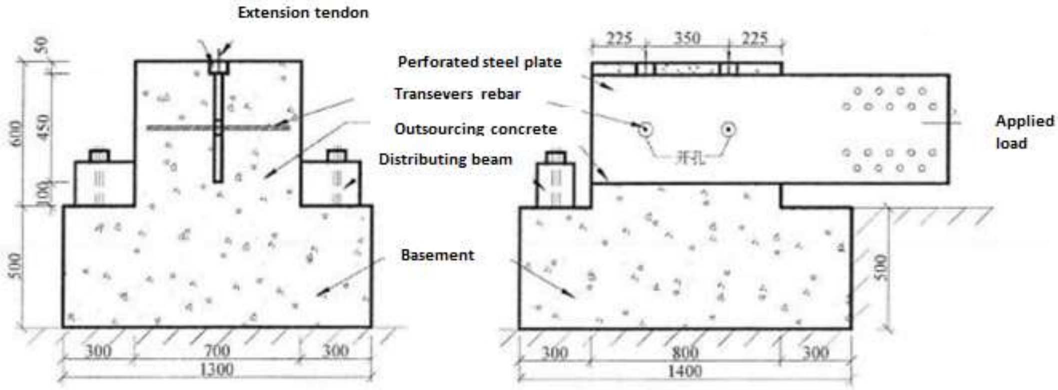

Figure 1 General structural diagram of the first test model (unit: mm)

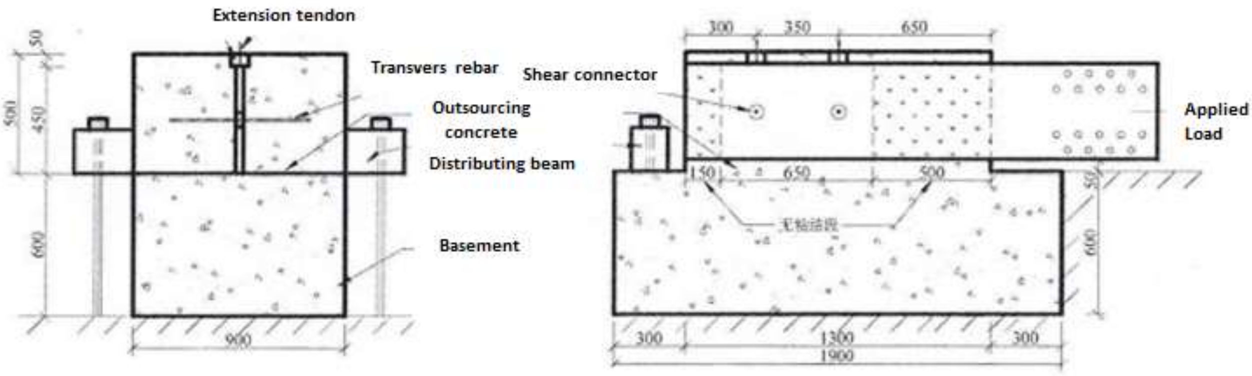

Figure 2 second test A60-20 -2D model structure diagram (unit: mm)

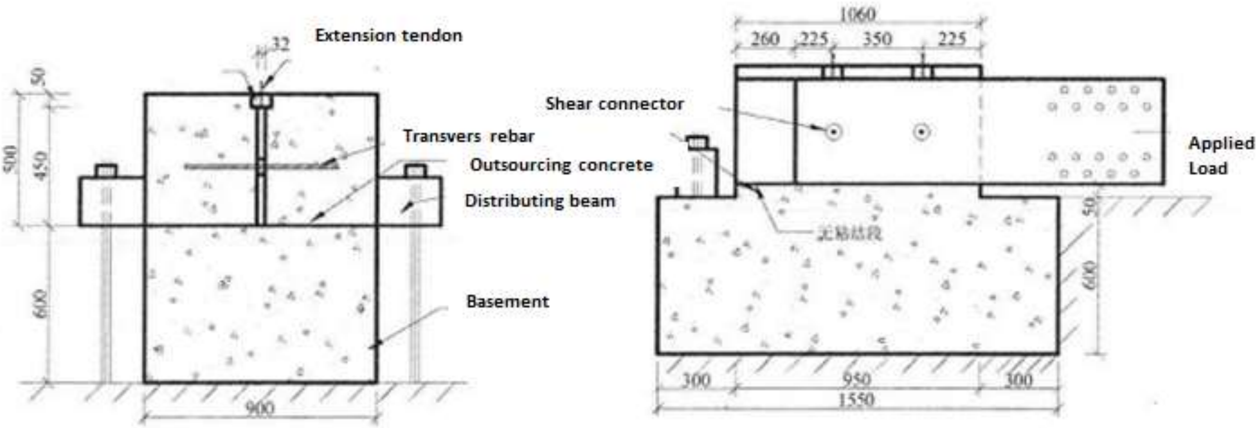

Figure 3 second test A45-16-2D model structure diagram (unit: mm)

ISSN 2055-6578(Print), ISSN 2055-6586(online)

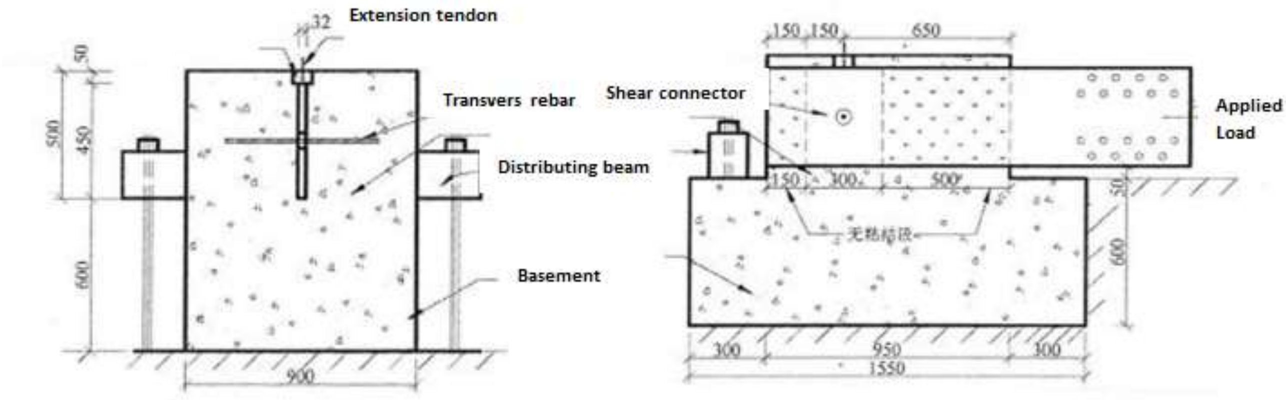

Figure 4 General structural diagram of the second test single shear bond model (unit: mm)

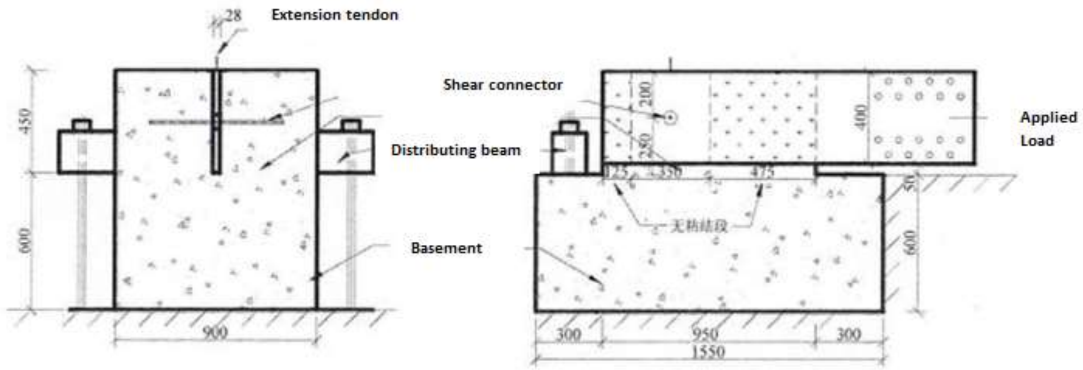

Figure 5 General structural diagram of the third test model (unit: mm)

\The test piece of the first test set two shear resistances, along with the loading direction. The concrete block of the base and the shear connector area is shallow as a whole, and its function is to provide shear boundary conditions for the concrete block in the shear connector area. The test pieces of the second test are divided into two types: Test pieces with two shear connectors in the loading direction, that is, test piece numbers with "D"; Single shear force test pieces, with test piece number "S." The test piece of the third test was the A60-20-3S test piece with the determined parameters.

Design of ordinary steel bar in model

The type of force applied to the test piece is similar to the short cantilever beam with the base protruding upward.

Using this method to calculate and arrange ordinary steel bars as shown in Figure 6 to Figure 10 shows. Moreover, the reinforcement ratio of the ordinary steel bars of the second and third tests was significantly lower than that of the first test. Except for the inner reinforcement of the shear connector, no other steel bars appeared on both sides of the steel plate at the same time.

ISSN 2055-6578(Print), ISSN 2055-6586(online)

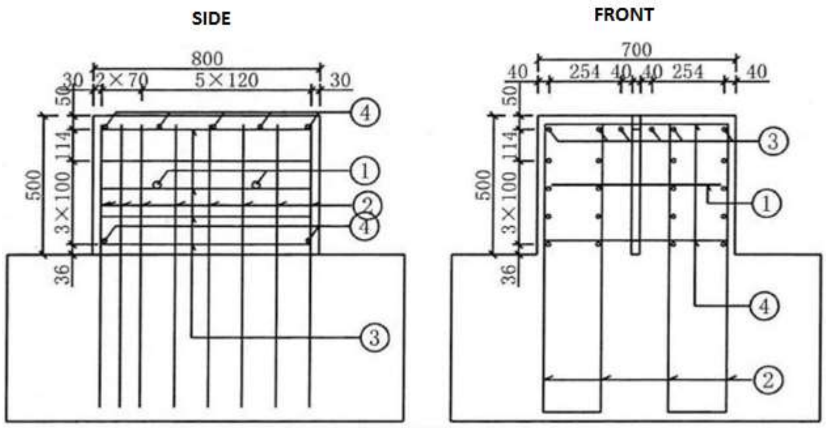

Figure 6 Reinforced steel structure of the first test

(N1 steel bar is the shearing force through the steel bar, N4 steel bar is ϕ12, the rest are all ϕ16)

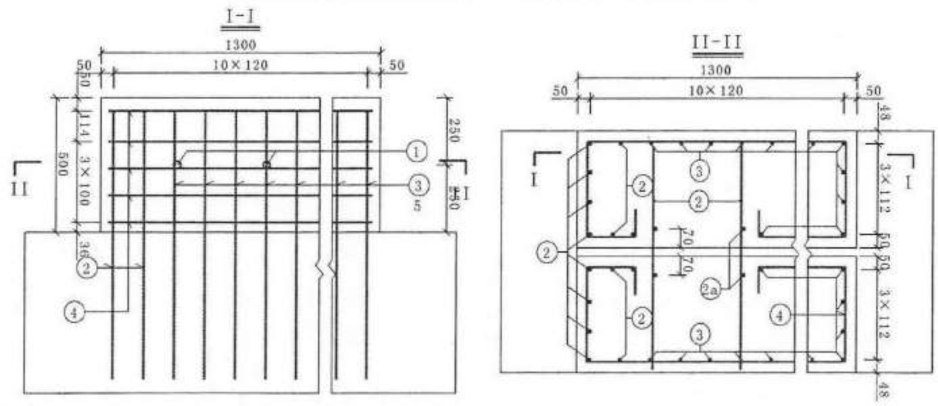

Figure 7 Reinforcement structure of A60-20-2D specimen in the second test

(N1 steel bar is the shearing force through the steel bar, N2 steel bar is ϕ16, the rest are ϕ12)

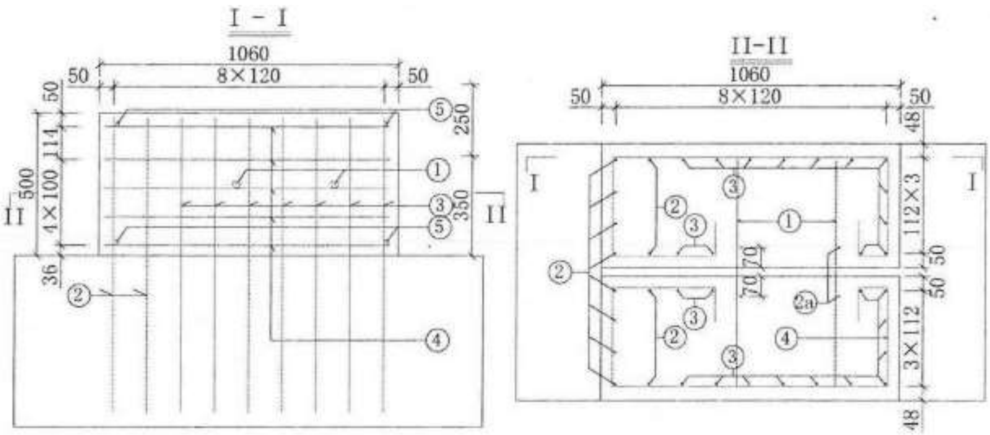

Figure 8 Reinforcement of A45-16-2D specimen in the second test

(N1 steel bar is the shearing force through the steel bar, N2 steel bar is ϕ16, the rest are ϕ12)

ISSN 2055-6578(Print), ISSN 2055-6586(online)

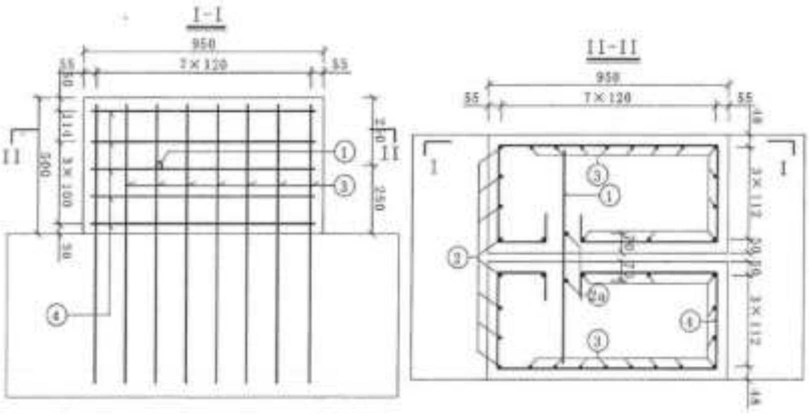

Figure 9 Single shear bond test piece reinforcement construction in the second test

(N1 steel bar is the shearing force through the steel bar, N2 steel bar is ϕ16, the rest are ϕ12)

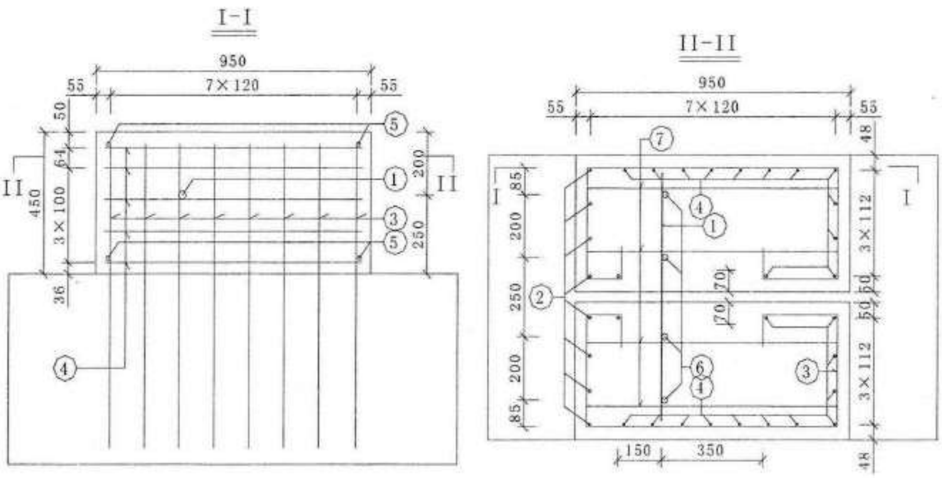

Figure 10 configuration of concrete block reinforcement in the third test

The other materials and geometric parameters of the model can be summarized as shown in Table 1.

Table 1 Main parameters of the shear bond test specimen

Specimen number	f_{yk} (MPa)	$f_{cu,k}$ (MPa)	D (mm)	d (mm)	p(%)	T (mm)	Number of Shear connector	Remarks
60-16-ID-1	335	45.4	60	16	3.090	32	2	First time
A60-16-I D-2	335	45.4	60	16	3.090	32	2	First time
A60-16-ID-3	335	45.4	60	16	3.090	32	2	First time
A45-16-ID-1	335	45.4	45	16	3.090	32	2	First time
A45-16-ID-2	335	45.4	45	16	3.090	32	2	First time
A45-16-ID-3	335	45.4	45	16	3.090	32	2	First time
A60-20-2S-1	335	45.4	60	20	1.429	32	1	Second time
A60-20-2S-2	335	45.4	60	20	1.429	32	1	Second time
A60-20-2S-3	335	28.4	60	20	I .429	32	1	Second time

ISSN 2055-6578(Print), ISSN 2055-6586(online)

A45-16-2D-1	335	29.6	45	16	1.399	32	2	Second time
A45-16-2S-1	335	29.6	45	16	1.399	32	1	Second time
A45-16-2S-2	335	29.6	45	16	1.399	32	1	Second time
A45-16-2S-3	335	29.6	45	16	1.399	32	1	Second time
A60-20-2S-1	335	44.0	60	20	2.188	28	1	Third time
A60-20-2S-2	335	44.0	60	20	2.188	28	1	Third time
A60-20-2S-3	335	44.0	60	20	2.188	28	1	Third time
A60-20-2S-4	335	44.0	60	20	2.188	28	1	Third time
A60-20-2S-S	335	44.0	60	20	2.188	28	1	Third time
A60-20-2S-6	335	44.0	60	20	2.188	28	1	Third time
A60-20-2S-7	335	44.0	60	20	2.188	28	1	Third time
A60-20-2S-8	335	34.2	60	20	2.188	28	1	Third time
A 60-20-2S-9	335	34.2	60	20	2.188	28	1	Third time

Where:

f_{yk} = is the standard value of yield strength of perforated steel.

$f_{cu,k}$ = is the standard value of cubic compressive strength of concrete.

D = is the diameter of perforated steel.

P= is the volume of common steel,

d =is the diameter of the transverse rebar,

t= is the thickness of perforated steel.

Test results and analysis

The load-slip curve of the first test specimen is shown in Figure 11and Figure 12 shows that

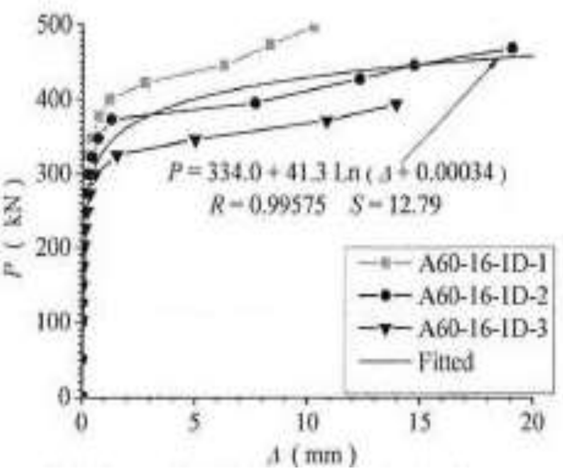

Figure 11 A60-16-1 D load-slip curve

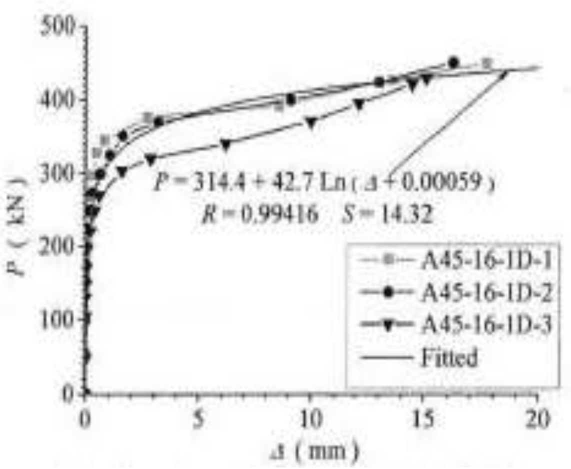

Figure 12 A45-16-1D load-slip curve

Where:

P =is the load on the single-hole shear connector

Δ= is the slippage of the open-hole steel plate relative to the concrete.

R= is the correlation coefficient of the regression analysis.

S= is the standard deviation.

ISSN 2055-6578(Print), ISSN 2055-6586(online)

For the first test load-slip curve, the results of the regression analysis are shown by the solid red line in Figure 11 and Figure 12.

In figure 13 shows a typical load-slip curve plot based on the first test data. The load-slip curve of the second test specimen is shown in Figure 14.

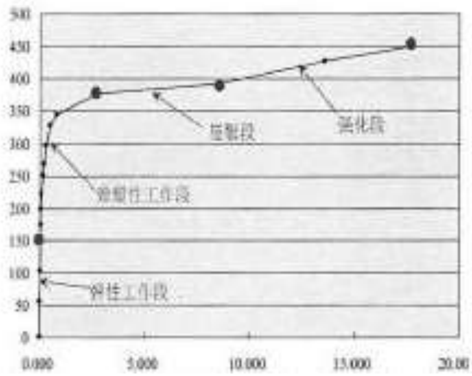

Figure 13 First test typical slip curve

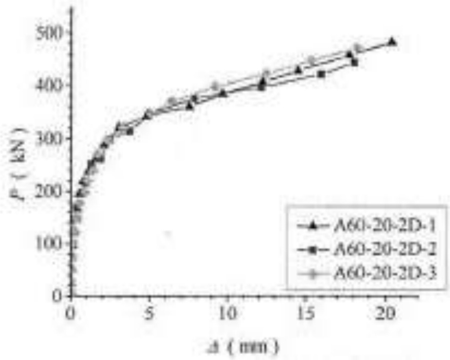

Figure 14 A60-20-2D load-slip curve

Figure 15 to 16 shows the load-slip curve obtained from the third test piece as shown in Figure 17 to Figure 18 shows.

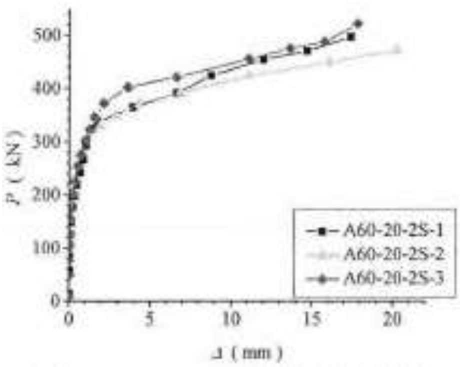

Figure 15 A60-20-2S load-slip curve

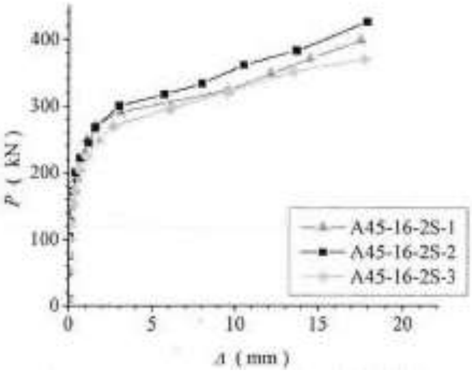

Figure 16 A45-16-2S load-slip curve

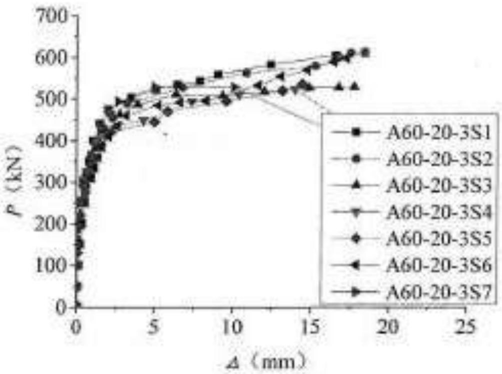

Figure 17 A60-20-3S-I~7 load-slip curve

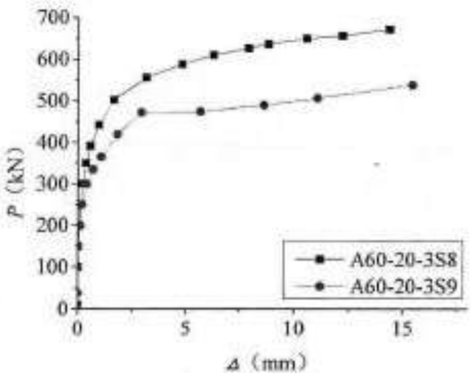

Figure 18 A60-20-3S-8~9 load-slip curve

ISSN 2055-6578(Print), ISSN 2055-6586(online)

According to the characteristics of the load-slip curve obtained by the test, the working state of the embedded PBL shear bond can be divided into the pseudo-elastic segment, elastoplastic segment, yielding phase and strengthening segment.

The test results show that in the pseudo-elastic working section, the slope of the curve is large, which is close to a straight line and the load can be considered to be linear with the slip. Correspondingly, in the initial stage of loading, the source concrete and transverse rebar are in a linear elastic working state, and the concrete is well-floating, and no cracks or damage are found. The applied load is mainly borne by the concrete zone and the transverse rebar.

As the amount of slip increases, the shear button enters the elastoplastic working segment. At this time, the crack on the concrete is gradually developed, so that the concrete stiffness is reduced, and the load is gradually transferred from the concrete to the transverse rebar. This appears as a decrease in the slope of the load-slip curve. When the crack gradually develops into the through the crack of the shearing surface of the concrete, the concrete is broken, and the shear bond yields.

The shear bond entering the yielding stage, the load is mainly borne by transverse rebar, so the stiffness is lower than the pseudo-elastic working section. At the same time, as the concrete dowel is cut, the shear section is rough, and in a Three-dimensional state of stress, so the aggregate on the shear section will bite and rub each other, and this interface action can also bear part of the load. In this stage, transverse rebar also gradually yield.

The load is transferred mainly through the interlocking friction of the aggregate in the concrete drop section.

This bearing mechanism has a certain degree of dispersion and randomness, after the yielding stage, the load-slip curve of some specimens shows obvious reinforcement phenomenon, while that of some specimens is not obvious.

Ultimate Bearing Capacity Study

The failure mode of the embedded PBL shear bond can directly exhibit its mechanical behavior and can be carried**;** the basis of the force limit state provides a basis.

Summarize and exemplify the failure modes of the three test pieces, as shown in Figure 19 to Figure 28 as shown below.

ISSN 2055-6578(Print), ISSN 2055-6586(online)

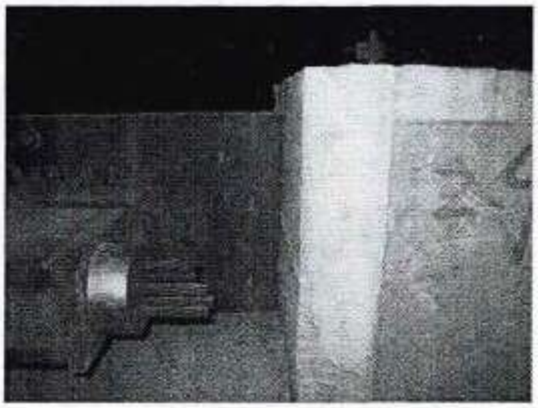

Figure 19 A60-16-1 D steel plate is pulled out

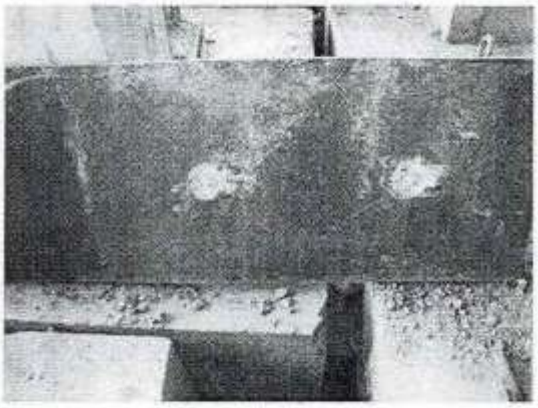

Figure 20 A60-16-ID steel plate on the concrete zen fracture

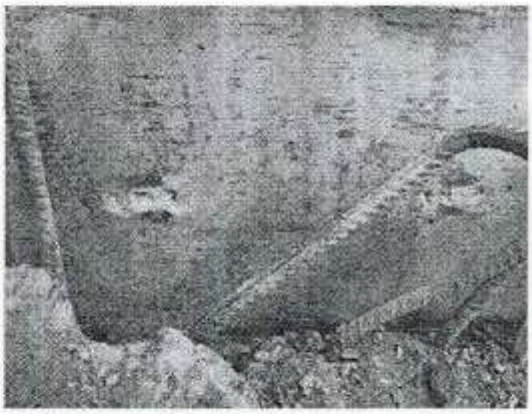

Figure 21 A45-16-1D concrete surface fracture

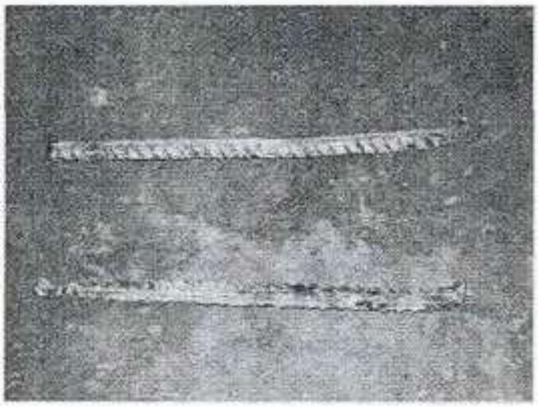

Figure 22 A45-16-1D transvers rebar

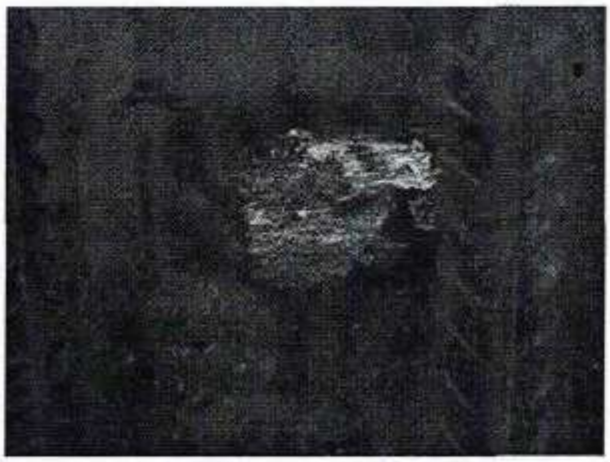

Figure 23 A60-20-2S concrete surface fracture

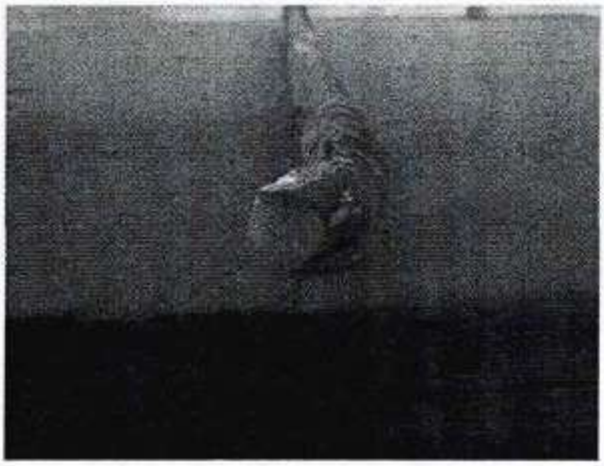

Figure 24 A60-20-2S transvers rebar fracture diagram

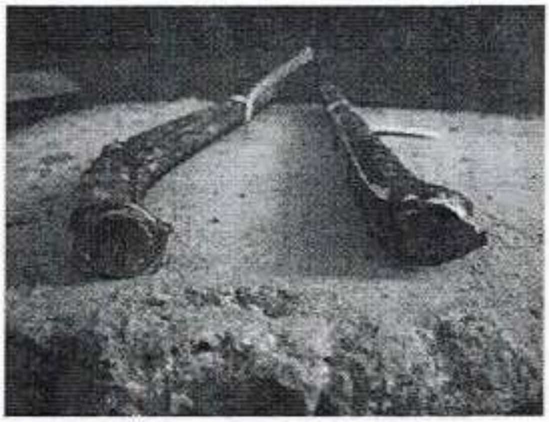

Figure 25 A45-16-2D transvers rebar fracture

Figure 26 A45-16-2S concrete surface section

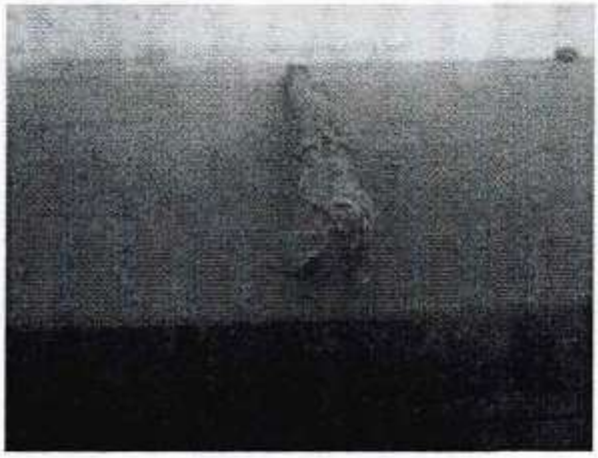

Figure 27 A45-16-2S transvers rebar fracture diagram

Figure 28 A45-16-2S concrete surface section

In the failure mode shown in the figure, the reinforced concrete is sheared; the through-reinforcing bar has been cut, and the two sections of the steel bar near the steel plate surface are flat shear failure surfaces within the thickness of the steel plate through steel.

The ribs also experienced severe bending deformation the open-hole steel plate and the concrete wall have obvious friction marks, the concrete in the steel plate opening is relatively intact, and the concrete block break is relatively flat.

SUMMARY

This part mainly introduces the test of the main cable misalignment system of the Nanjing Yangtze River Fourth Bridge, introduces the test situation.

The results of the test were analyzed and summarized. The main conclusions are as follows:

ISSN 2055-6578(Print), ISSN 2055-6586(online)

1) The specific geometric parameters and reinforcement of the test piece in the test are introduced. The geometry and material parameters required for modeling can be provided for the establishment of the finite element model.

2) The load slip curves obtained from the test are summarized, the load-bearing process of the embedded PBL shear bond can be divided into the quasi-elastic working segment, elastoplastic working segment, yielding phase and strengthening phase, the bearing mechanism of each phase is summarized.

3) The ultimate bearing capacity of the embedded PBL shear bond defined by the test is the load value under the slip of 10 mm, and there is a certain degree of human subjectivity. According to the bearing mechanism and bearing characteristics, the ultimate bearing capacity is defined as the corresponding load value when the full section of the steel is yielded; it has considerable theoretical significance and is also consistent with the characteristics of engineering use.

4) In order to facilitate the observation of the yielding stage of the steel bar during the load-bearing process of the shear connector, finite element model analysis is needed to verify and analyze.

METHODOLOGY

The model test of the embedded PBL shear bond often only obtains some macroscopic mechanical characteristics, such as the final load value during loading, the load-slip relationship, and the final failure mode. For internal components such as concrete zone and through steel bars, the process of gradual development from damage to failure during loading and the variation of internal complex stress cannot be obtained through experiments. If the state of yielding through the full section of the steel bar is taken as the bearing capacity limit state of the shear connector, a fine finite element model needs to be established. Through the macroscopic mechanical characteristics obtained by the experiment and the meso-mechanical behavior calculated by the fine finite element theory model, the bearing mechanism of the shear bond can be deeply grasped, which can provide a theoretical basis for the determination of the ultimate state of the bearing capacity of the shear bond.

The concrete zone and the peripheral source concrete of the embedded PBL shear connector are in complex three-dimensional stress. The shearing and damage process of the concrete zone and the surrounding concrete are also the difficulties and connector points of the finite element simulation, so the reasonable concrete is used. Constructing a model is the connector to avoiding finite element model simulation distortion. However, traditional fine finite element model calculations generally have problems such as low computational efficiency and high equipment requirements. Therefore, it is also important to select suitable finite element software and calculation methods to solve the problem. In this paper, the finite element simulation of each test piece in the test of the main cable laying system of the Nanjing Yangtze River Bridge is carried out by the nonlinear finite element software ABAQUS.

The idea of this part based on the damage characteristics of a concrete wave in the embedded PBL shear connector and the characteristics of interface friction and occlusion, the finite element software ABAQUS with strong nonlinear computing ability is selected.

ISSN 2055-6578(Print), ISSN 2055-6586(online)

The constitutive relation is used as the constitutive model of the computational model, according to the geometric model of the model test as above.

Reinforcement, material parameters, etc., establish a fine ABAQUS finite element model. In order to select a solution method that can quickly avoid the simulation distortion problem, the simulation calculations are compared with different solvers in the software to determine the most suitable solution method.

- **Selection of material parameters:**
- **Constitutive transverse rebar**

During the loading process of the embedded PBL shear connector, the stress of the concrete swing is complicated, and the calculation does not converge.

To facilitate the calculation convergence, the constitutive structure of the transverse rebar does not consider the damage, and the trilinear isotropic strengthening model is adopted. The elastic modulus is 206000 MPa, and the Poisson's ratio is 0.28. The user needs to input the plasticity parameters, as shown in Table 2. The relationship between yield stress and plastic strain is shown in Figure 29.

Table 2 shows the plastic parameters of transverse rebar

Yield stress σ (MPa)	**Plastic strain ε^{pl}**
335	0
445	0.00449

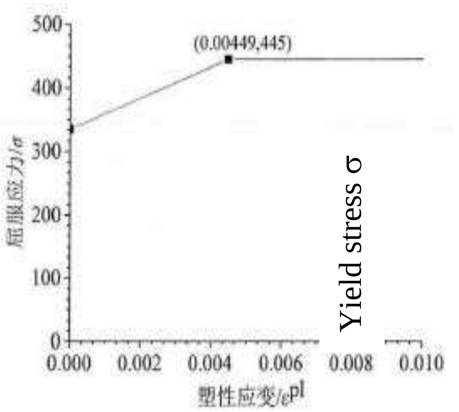

Figure 29 Constitutive curve transvers bar

Plastic strain ε^{pl}

- **Constitutive of concrete**

The elastic modulus is determined according to the literature, and the Poisson's ratio is uniformly selected as 0.18. In the damage plasticity model of ABAQUS, the user also needs the plasticity of the material input parameters, after debugging, can be selected as shown in Table 3.

During the trial calculation, it is found that the dilatancy angle @ and the viscosity coefficient U have a great influence on the calculation results, and determine whether the model converges or not. These two parameters have been discussed in detail in references, so the impact of this parameter will not be discussed in this paper.

Table 3Plastic damage plasticity model material plastic parameters.

Dilation Angle	Eccentricity	Fb0/fco	K	Viscosity parameter
30	0.1	1.16	2/3	0.0005

In the damage plasticity model, it is also necessary to input the compressive yield stress-compression inelastic strain (σ_c - $\varepsilon_c^{\sim in}$) data in the form of a table, compressive damage variable-compressed inelastic strain (d_c - $\varepsilon_c^{\sim in}$) data.

Yielding should be - tensile cracking strain (σ_t - $\varepsilon_t^{\sim ck}$) data, tensile damage variable - tensile cracking strain (d_t - $\varepsilon_t^{\sim ck}$) data.

According to the test part which was mentioned in the test part, the basic parameters of the concrete of each test piece can be determined from Table 1.

The compressive strength of the concrete cube to be calculated is 45.4 MPa, 28.4 MPa, 29.6 MPa, 44 MPa, and 34.2 MPa, the data required for the above concrete damage models in ABAQUS can be calculated, as shown from Table4 to Table 8.

Table 4 Parameter of the concrete CDP model with cube strength of 45.4 MPa

Compressive strength $\boldsymbol{\sigma_c}$ (Mpa)	Compressed inelastic strain $\boldsymbol{\varepsilon_c^{\sim in}(x10^{-3})}$	Pressure damage $\boldsymbol{d_c}$	tensile strength $\boldsymbol{\sigma_t}$ (Mpa)	Tensile inelastic $\boldsymbol{\varepsilon_t^{\sim ck}(x10^{-3})}$	Tensile damage $\boldsymbol{d_t}$
20.89	0	0	2.67	0	0
29.88	0.753	0.265	2.54	0.032	0.164
27.86	1.24	0.368	2.2	0.069	0.303
24.07	1.78	0.465	1.8	0.108	0.425
20.42	2.315	0.545	1.49	0.144	0.516
17.38	2.832	0.608	1.27	0.177	0.582
14.97	3.33	0.657	1.1	0.209	0.633
13.06	3.813	0.696	0.88	0.269	0.703
11.54	4.285	0.728	0.64	0.384	0.784
9.77	4.976	0.766	0.43	0.605	0.857
7.9	5.989	0.806	0.28	1.039	0.912
6.1	7.478	0.846	0.17	1.9	0.948
4.53	9.674	0.883	0.11	3.616	0.97
2.8	14.806	0.925	0.07	7.037	0.983

Table 5 Parameter of the concrete CDP model with cube strength of 28.4 MPa

Compressive strength $\boldsymbol{\sigma_c}$ (Mpa)	Compressed inelastic strain $\boldsymbol{\varepsilon_c^{\sim in}(x10^{-3})}$	Pressure damage $\boldsymbol{d_c}$	tensile strength $\boldsymbol{\sigma_t}$ (Mpa)	Tensile inelastic $\boldsymbol{\varepsilon_t^{\sim ck}(x10^{-3})}$	Tensile damage $\boldsymbol{d_t}$
13.3	0	0.000	2.03	0	0.000
19.02	0.798	0.33	1.93	0.027	0.156

ISSN 2055-6578(Print), ISSN 2055-6586(online)

17:49	1.475	0.463	1.78	0.055	0.276
14.98	2.184	0.564	1.56	0.086	0.381
12.74	2.884	0.638	1.37	0.115	0.462
10.95	3.569	0.692	1.22	0.144	0.526
9.54	4.24	0.733	1	0.198	0.616
8.42	5	0.764	0.75	0.299	0.719
7.52	5.553	0.79	0.52	0.493	0.814
6.47	6.521	0.819	0.34	0.87	0.885
5.34	7.957	0.85	0.22	1.615	0.932
4.22	10.087	0.881	0.14	3.1	0.961
2.86	14.791	0.919	0.09	6.058	0.978

Table 6 Parameter of the concrete CDP model with cube strength of 29.6 MPa

Compressive strength σ_c (Mpa)	Compressed inelastic strain $\varepsilon_c^{\sim in}(x10^{-3})$	Pressure damage d_c	tensile strength σ_t (Mpa)	Tensile inelastic $\varepsilon_t^{\sim ck}(x10^{-3})$	Tensile damage d_t
13.86	0	0	2.08	0	0
19.83	0.796	0.324	1.98	0.027	0.157
18.26	1.445	0.453	1.82	0.056	0.279
15.66	2.129	0.554	1.58	0.088	0.385
13.31	2.804	0.629	1.39	0.118	0.467
11.43	3.463	0.624	1.23	0.147	0.531
9.94	4.109	0.725	1.1	0.174	0.581
8.77	4.743	0.758	0.92	0.228	0.654
7.82	0.464583	0.784	0.7	0.329	0.741
6.72	6.298	0.814	0.49	0.524	0.825
5.53	7.673	0.846	0.?3	0.906	0.89
4.36	9.712	0.878	0.21	1.662	0.934
2.83	14.793	0.92	0:14	3.166	0.962

Table 7 Parameter of the concrete CDP model with cube strength of 44 MPa

Compressive strength σ_c (Mpa)	Compressed inelastic strain $\varepsilon_c^{\sim in}(x10^{-3})$	Pressure damage d_c	tensile strength σ_t (Mpa)	Tensile inelastic $\varepsilon_t^{\sim ck}(x10^{-3})$	Tensile damage d_t
20.34	0	0	2.63	0	0
29.09	0.757	0.269	2.63	0.032	0.163
27.1	1.251	0.373	2.18	0.068	0.301
23.41	1.796	0.471	1.79	0.107	0.422
19.86	2.336	0.55	1.49	0.142	0.512
16.92	2.858	0.612	1.27	0.175	0.579

ISSN 2055-6578(Print), ISSN 2055-6586(online)

14.58	3.362	0.661	0.98	0.237	0.669
12.73	3.851	0.7	0.69	0.353	0.766
11.25	4.329	0.732	0.45	0.573	0.849
9.53	5.031	0.769	0.28	1.004	0.908
7.72	6.059	0.809	0.18	1.859	0.947
5.97	7.571	0.848	0.11	3.562	0.97
4.44	9.803	0.885	0.07	6.957	0.983
2.79	14.805	0.925	0.04	13.71	0.99

Table 8 Parameter of the concrete CDP model with cube strength of 34.2 MPa

Compressive strength $\boldsymbol{\sigma_c}$ (Mpa)	Compressed inelastic strain $\boldsymbol{\varepsilon_c^{\sim in}(x10^{-3})}$	Pressure damage $\boldsymbol{d_c}$	tensile strength $\boldsymbol{\sigma_t}$ (Mpa)	Tensile inelastic $\boldsymbol{\varepsilon_t^{\sim ck}(x10^{-3})}$	Tensile damage $\boldsymbol{d_t}$
20.89	0	0	2.67	0	0
29.88	0.753	0.265	2.54	0.032	0.164
27.86	1.24	0.368	2.2	0.069	0.303
24.07	1.78	0.465	1.8	0.108	0.425
20.42	2.315	0.545	1.49	0.144	0.516
17.38	2.832	0.608	1.27	0.177	0.582
14.97	3.33	0.657	1.1	0.209	0.633
13:06	3.813	0.696	0.88	0.269	0.703
11.54	4.285	0.728	0.64	0.384	0.784
9.77	4.976	0.766	0.43	0.605	0.857
7.9	5.989	0.806	0.28	1.039	0.912
6.1	7.478	0.846	0.17	1.9	0.948
4.53	9.674	0.883	0.11	3.616	0.97
2.8	14.806	0.925	0.07	7.037	0.983

- **Finite element model of embedded PBL shear connector**

Considering the symmetry of the model specimens, in order to save the computational cost, a 1/2 model is established for simulation analysis. In order to simulate the behavior of the shear connector to continue to be carried after being sheared, the displacement of the front end of the steel plate is 3 mm, corresponding to the test, as shown in Figure 30.

The model is mainly composed of four parts:

1- Concrete block.

2- Transverse rebar.

3- open-hole steel plate.

4- Ordinary steel bar.

ISSN 2055-6578(Print), ISSN 2055-6586(online)

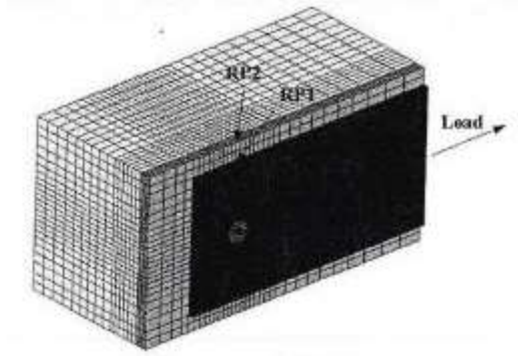

a) 1/2 overall model diagram

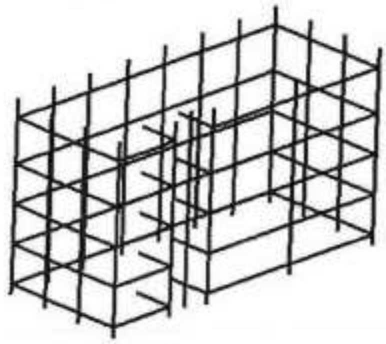

b) ordinary steel bars

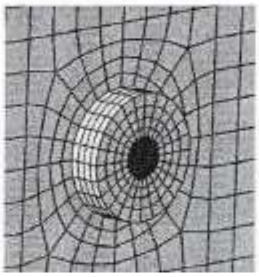

C) Concrete dowel

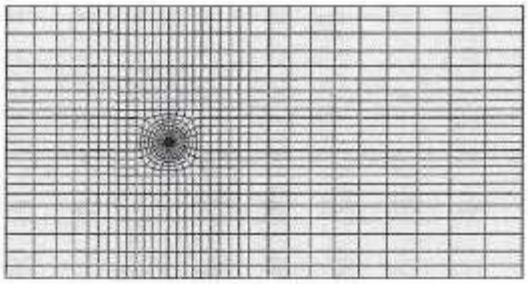

d) concrete block front

e) transverse rebar

F) Open hole steel plate

Figure 30 Model Mesh Map

The common reinforcement is simulated by the linear truss element (T3D2). The three-dimensional truss element is only stressed in the axial direction but not in the tangential direction, while the other parts are all three-dimensional solid units. When fully integrated units (C3D8 and C3D20) of three-dimensional solid units are subject to bending, shear locking phenomenon is easy to occur, which makes the units too rigid.

The computational accuracy of the units is poor even if they are divided into very thin grids.

The non-coordination unit (C3D8I) can avoid the problem of shear self-locking, and the calculation cost is much lower than that of the secondary unit, while the accuracy is very close to that of the secondary unit. However, C3D8I depends on the shape of the unit, and a good quality hexahedral mesh is needed to obtain satisfactory calculation accuracy.

Therefore, the three-dimensional linear reduction integration unit (C3D8R) is used for the concrete block, the through-reinforcing steel and the open-hole steel plate. This unit has one integration point in each direction than the complete integration unit, so the calculation efficiency is high, but the reduction integral unit There is a numerical problem of(hourglassing), that is, the mode in which the unit is in zero energy when bending, and the effect of the hourglass can be eliminated by the algorithm of the enhanced hourglass control, and the subdivision grid is used to eliminate the influence of the calculation accuracy, and the unit Suitable for contact problems under large strains.

The mesh of the element should be refined appropriately according to the requirement. The mesh should be subdivided in the region near the concrete birch with concentrated local forces. At least four elements are distributed on the 90-arc. The steel plate thickness and the thickness direction of the concrete birch should not be less than four elements. The specific mesh division is shown in Figure 30.

- **Simulation of contact and boundary**

The simulation of the interaction is related to the calculation convergence and accuracy of the whole finite element model. The real boundary needs to be simulated, and other simplified measures should be considered to accelerate convergence. The interaction of embedded PBL shear bond is basically as follows:

1- Contact between ordinary steel bars and peripheral concrete blocks.

2- Contact between the transverse rebar and the concrete block.

3- Contact between the concrete structure in the hole and the thickness direction of the perforated steel plate.

4- Non-bonding contact between concrete and steel plate outside the open-hole steel plate surface.

5- The contact between the concrete and the bond section of the open-hole steel plate surface.

The simulation of contact (1) is to use the ordinary steel unit as a built-in unit, and the built-in area (Embedded region) constraint is built into the main unit of the concrete block. The calculation of this constraint only considers the relative displacement of the master-slave unit node to realize the slave node unit. The transformation of the stiffness matrix, the built-in area constraints can be used to show the calculation of steel and concrete separately in the post-processing. Contact (2) is the direct contact of the solid element. In the actual embedded PBL shear connector, the amount of slippage between the transverse rebar and the concrete block is small, which can be neglected, so that the joint between the transverse rebar and the concrete block can be shared. that is, the slip between the two is not considered. Contact (3), (4), (5) are the contact between steel plate and concrete, and the normal action is hard to contact, which means that the two do not penetrate each other, and both steel plates are used as the main surface, contact (5) It is also necessary to consider the tangential friction effect, using the penalty formula, setting the friction coefficient to 0.25, and contacting (3) and (4) only considering the normal effect.

The simulation of boundary conditions should be strictly based on the actual situation of the test. In the finite element model, the base of the peripheral concrete block is not simulated, and all the nodes of the peripheral concrete bottom surface are consolidated. Since the 1 /2 model is established, the symmetric boundary is adopted on the symmetry surface to limit the Z

ISSN 2055-6578(Print), ISSN 2055-6586(online)

degrees of freedom (that is, the direction perpendicular to the steel plate). The bottom surface of the steel plate is constrained in its Y direction (i.e., parallel to the steel plate and perpendicular to the direction of the applied tensile force) according to the test conditions. The model diagram after the boundary conditions is defined shown in figure 31.

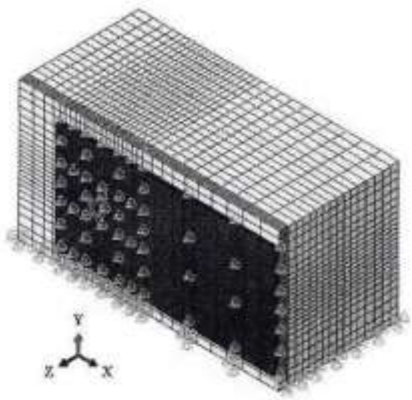

Figure 31 boundary condition simulation diagrams

According to the above, modeling of the finite element analysis of various embedded PBL shear connectors can be completed, and all the models are listed and summarized as shown in Figure 32.

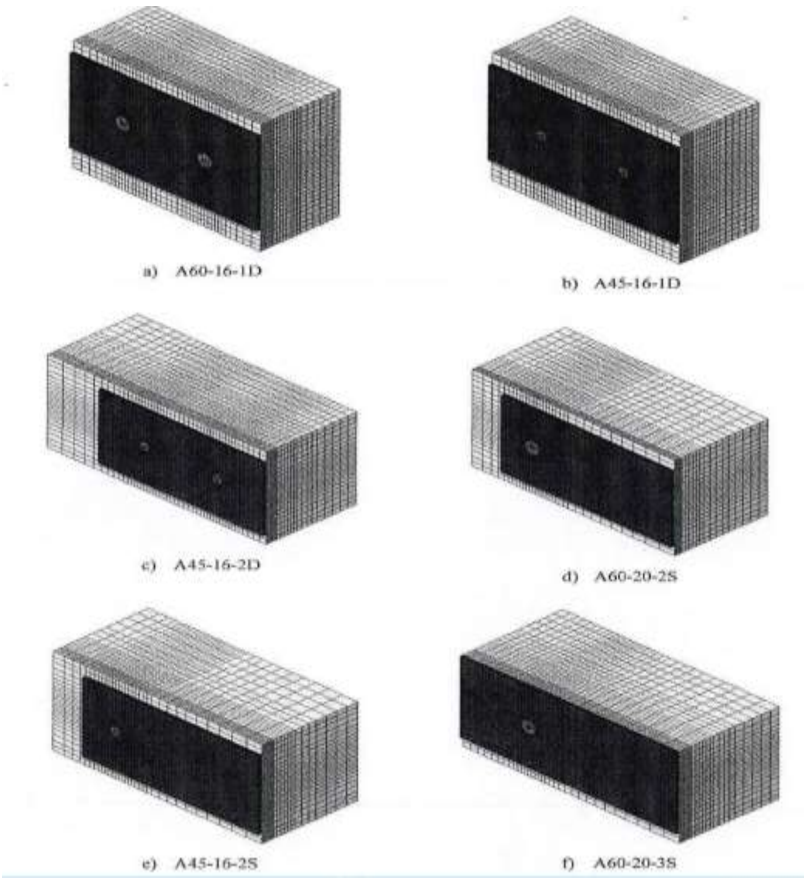

Figure 32 Summary of the finite element model

Calculation results and analysis

The purpose of using different nonlinear solution methods is mainly to determine a computational method with high computational efficiency and low cost. Therefore, it is necessary to consider the comparison between the calculation results and the test results, such as the comparison of the macro load-slip curve, the comparison of the shear bond failure modes, and the microscopic Component local stress and damage distribution, etc., to determine the reliability of the calculation method; also need to consider the calculation efficiency and other aspects.

- **Analysis of the results of nonlinear solution methods**

In order to observe the crack development of the structure, as shown in Figure 33, the crack propagation of concrete blocks and concrete is listed. Since there is no initial crack, the dynamic crack propagation of the model can be found. The crack is initially sprouted in the concrete. Nearby, and then along the direction of the loading angle of 45 °, the crack can arbitrarily pass through the inside of the unit, which is consistent with the experimental phenomenon (as shown in Figure 33).

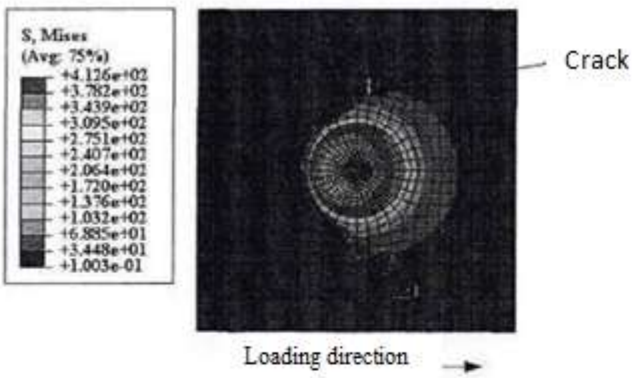

a) Cracking of wrapped concrete (MPa)

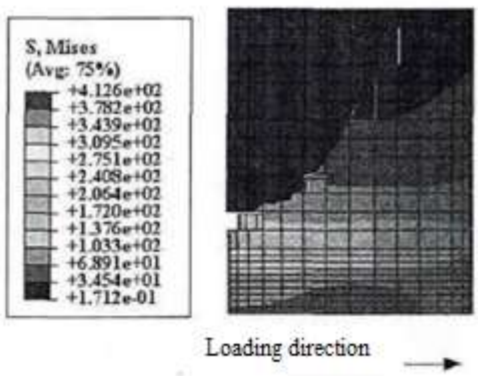

b) Cracking of concrete (MPa)

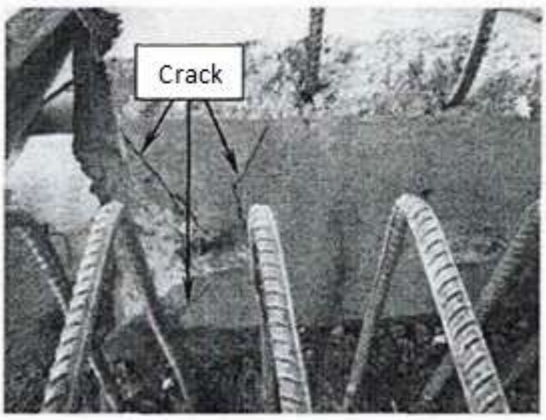

Figure 33 Modeling simulation results and test results

There are also some problems:

(1) The convergence problem of the model, under the displacement of 3mm displacement, the calculated slip amount is about 0.5mm;

(2) The extracted load-slip curve is quite different from the test result;

(3) The path of the crack expansion inside is not true, and the concrete wave is not cut as in the testing phenomenon.

- **Load-slip curve verification**

After the finite element model of each embedded PBL shear connector is established, the static general implicit solution method is used for analysis. To verify the reliability of the theoretical model, the load should be smoothed first. The shift curve is compared, which is the macroscopic phenomenon reflected in the calculation.

Compare the calculated load-slip curve of each finite element model with the experimental results, as shown in Figure 34.

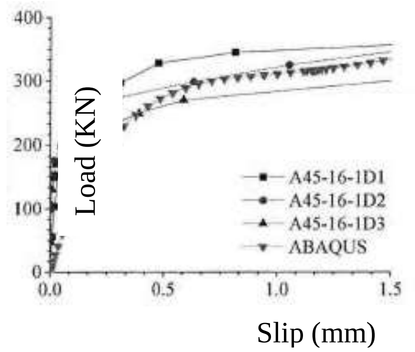

a) A45-16-Ld

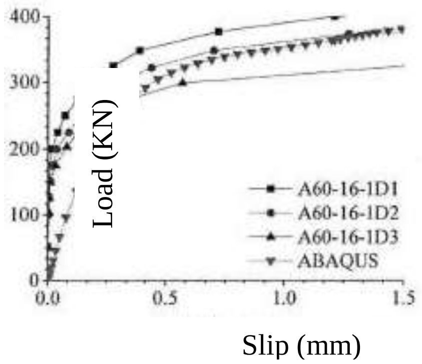

b) A60-16-lD

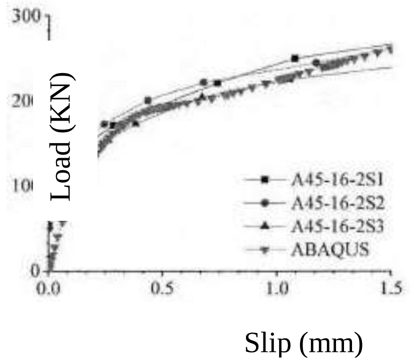

c) A45-16-2S

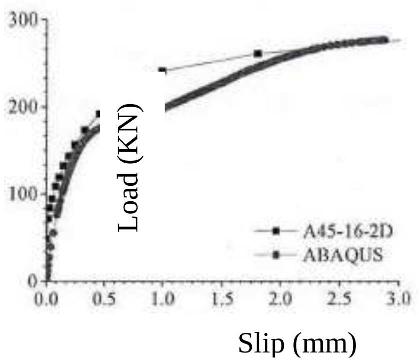

d) A45-16-2D

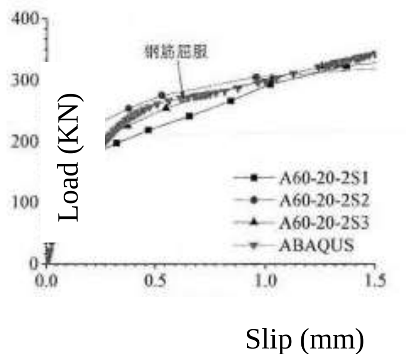

e) A60-20-2S

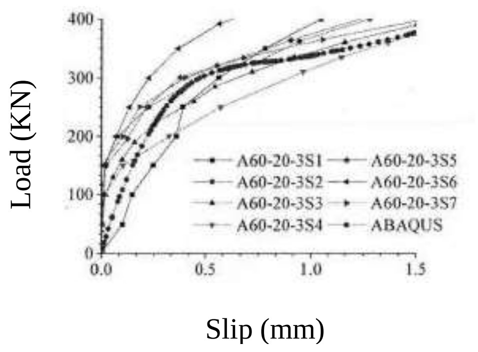

f) A60-20-3S-1~7

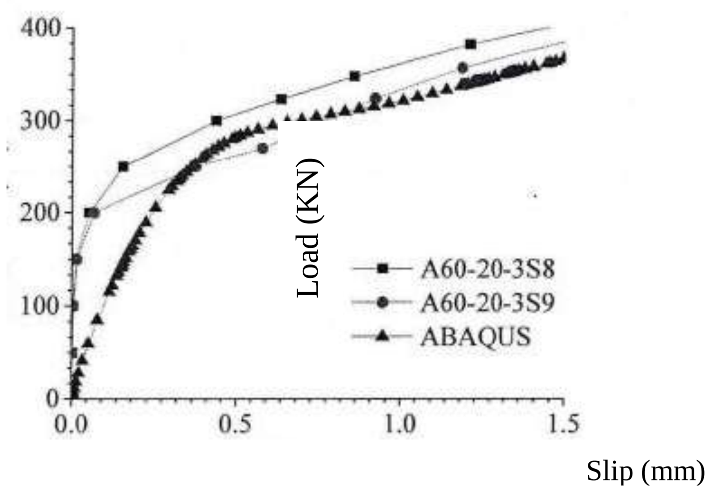

g) A60-20-3S-8~9

Figure 34 Comparison of the load-slip curve calculated by the theoretical model and the test results.

Comparing the curve cases in the graph, the analysis can obtain the following conclusions about the finite element model:

1) The load-slip curve obtained by the static general implicit solution method is very smooth throughout the calculation process, and there is no sudden or oscillating phenomenon. This is because the Hilber-Hughes-Tayloy algorithm used in this method is linear. The calculation of the system is unconditionally stable. In the solution process, even if linear displacement loading is used directly, the oscillation problem of the dynamic explicit algorithm will not occur; in the modeling process, because the amplification quality and increase are not needed The parameter setting such as material damping will not cause the noise phenomenon due to the overestimation of the inertial force or the increase of the material damping. Therefore, the static general analysis can more accurately reflect the force of the theoretical model, and the calculation accuracy is higher.

2) The curves calculated by the above finite element model all have the problem that the initial slope of the load-slip curve is smaller than the test value. It can be clearly seen that the load value increases when there is zero slip at the initial stage of the test curve,

ISSN 2055-6578(Print), ISSN 2055-6586(online)

which may be during the test, there was an initial bond between the perforated steel sheet and the concrete in the test piece, and this initial interface effect was destroyed as the loading gradually increased. In the finite element model, this interface effect is not simulated, so the slope of the initial curve of this loading is low.

3) The calculation curve agrees well with the test results, indicating that the method of finite element simulation is reliable. At the same time. The calculation formula of the damage variable derived by the Sidoroff energy equivalent principle is not only simple but also the calculation result. It is true and reliable, and it can well reflect the characteristics of stiffness degradation and plastic deformation caused by damage under concrete loading. These are macroscopic phenomena reflected by the damage plasticity model, and the microscopic phenomena calculated by this model will be detailed later.

4) The development of the test curve and the calculation curve in the figure is as follows: the slope of the initial curve is large, which means that the initial load-bearing stiffness of the shear bond is very large, and the slip is about 0.5 mm, and the stiffness starts to decrease significantly, but the load Force can continue to increase. It shows that the embedded PBL shear bond has its bearing capacity entering the next stage after the slip amount reaches about 0.5mm, which is consistent with the conclusion obtained in the experiment. With the increase of the load, the concrete dowel Damage occurs and gradually withdraws from work, resulting in reduced stiffness.

- **Failure form verification**

It can be seen from the overall stress diagram in Figure 35 that the stress is concentrated in the area around the shear bond, and the stress in most other areas is zero, which is related to the experimental phenomenon of the embedded PBL shear bond test (Figure 36) Consistent. The outer concrete is in good appearance. After the shear connector is opened, it can be found that although the outer concrete is intact, the concrete has been cut and the steel bar has undergone large deformation.

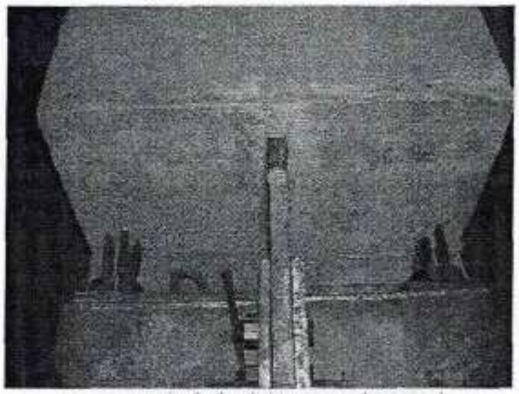

Figure 35 specimen front failure mode in the test

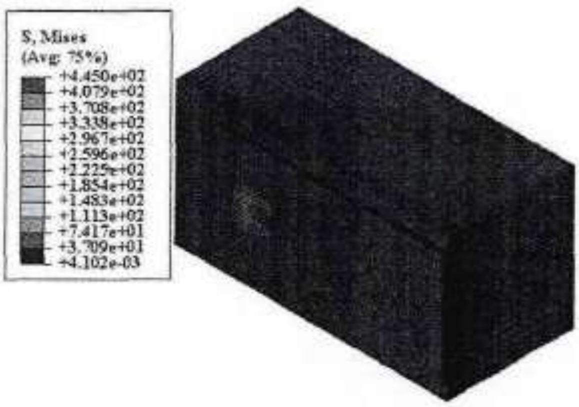

Figure 36 Whole diagram of ABAQUS model destruction form (MPa)

Under the shearing action of the thickness of the steel plate, the stress near the shear plane is the largest, and the stress of the steel bar away from the shear bond position gradually becomes smaller and closer to zero.

ISSN 2055-6578(Print), ISSN 2055-6586(online)

International Journal of Civil Engineering, Construction and Estate Management
Vol.6, No.4, pp.1-30, December 2018
Published by European Centre for Research Training and Development UK (www.eajournals.org)

These are the same as the actual force performance of the PBL shear connector, and the deformation of the transverse rebar after loading is also consistent with the testing phenomenon in Figure 37.

It can be clearly seen from the stress situation in Fig 38 that the steel bar running through the shear plane and the vicinity of the steel bar has already yielded the full section, indicating that the bearing mechanism of the shear bond has been degraded to rely on the interface of the bite and friction.

The effect is to carry because the plastic model is directly used without defining damage to the steel bar, the damage of the steel cannot be displayed.

Figure 37 failure mode of test specimen passing transvers rebar

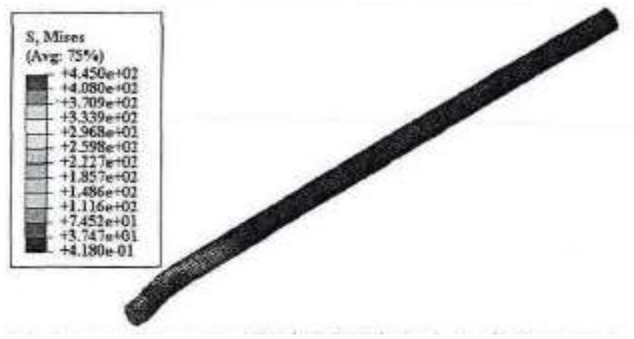

Figure 38 stress and deformation of steel bar in ABAQUS model

Figure 39 shows the stiffness coefficient degradation (SDEG) of the concrete dowel shear plane at 0.5 mm slip. At this time, most of the area has entered the stiffness degradation value of 70% and above, indicating the concrete dowel.

Gradually withdrawing from the work, the bearing mechanism gradually turned into the concrete dowel and the occlusion effect of the steel bar and the interface.

After a slip of 0.5 mm, the load of the shear connector enters the next stage of work due to the shearing of the concrete sample.

Figure 40 shows the stiffness degradation coefficient (SDEG) of the shear plane at the concrete sample at the concrete/steel interface. The stiffness degradation coefficient of the concrete dowel contact surface is 99%, near the shear bond.

The coefficient of stiffness degradation of other concrete decreases rapidly with the position away from the shear bond.

ISSN 2055-6578(Print), ISSN 2055-6586(online)

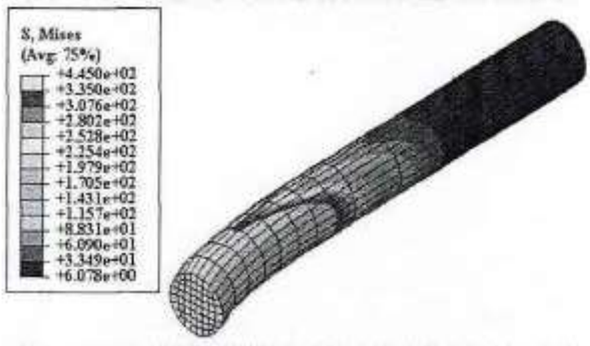

Figure 39 stress diagram near the shear surface of transvers rebar (MPa)

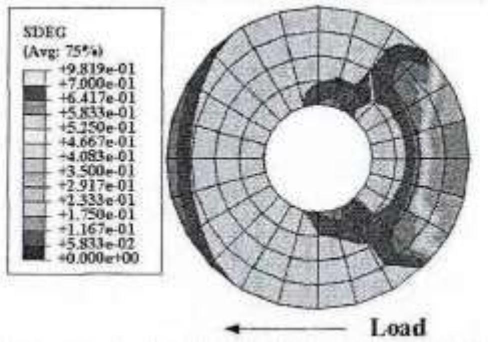

Figure 40 stiffness degradation of 0.5mm sliding concrete shear surface

Figure 41 Shear bond on the steel plate in the test

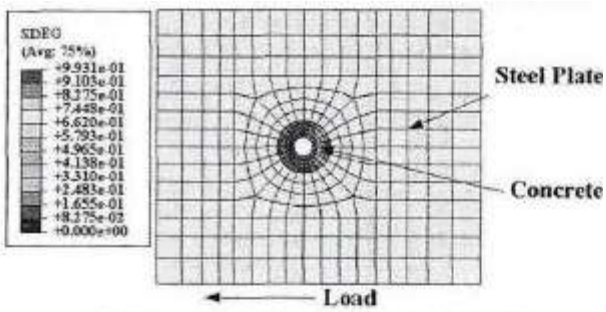

Figure 42 Stiffness Degradation of Shear Bonds on Steel Plates

Figure 43 shows the shearing of the shear bond on the concrete surface of the test. The concrete around the shear bond is mostly intact. Figure 42 shows the concrete within the thickness of the perforated steel plate.

The sample of the stiffness degradation coefficient (SDEG) is the same as the phenomenon of the shear bond on the steel plate obtained by the test. The results of the finite element analysis are almost consistent with the experimental results.

In order to compare with the experimental phenomenon, the stress map of the perforated steel plate was extracted from the finite element model.

It can be clearly seen in Figure 46 that the steel plate did not yield, which is consistent with the condition of the steel plate extracted after the test.

The stress map of the steel frame simulated by the T3D2 analysis unit can clearly show that the reinforcement of the steel frame is small, the maximum stress is only 25 MPa, and the stress is concentrated near the position of the shear connector.

The ordinary steel bars on the steel plate side near the shear connector and the loading direction have the greatest stress. Figure 48 shows the displacement diagram of the concrete.

The deformation in the figure further shows that the deformation of the concrete near the concrete is small.

ISSN 2055-6578(Print), ISSN 2055-6586(online)

Therefore, most of them are relatively complete, and the simulation results are consistent with the experimental phenomena.

Figure 43 Shear force fracture on the concrete surface in the test

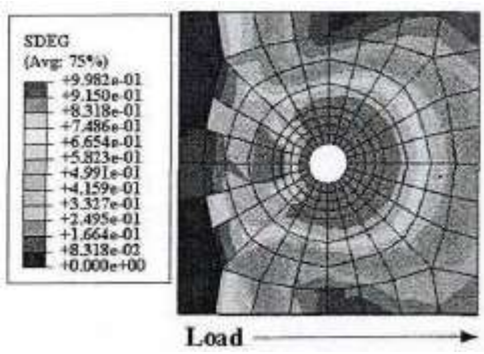

Figure 44 Deformation of fracture stiffness of shear bond on concrete surface

Figure 45 The open-hole steel plate drawn from the test

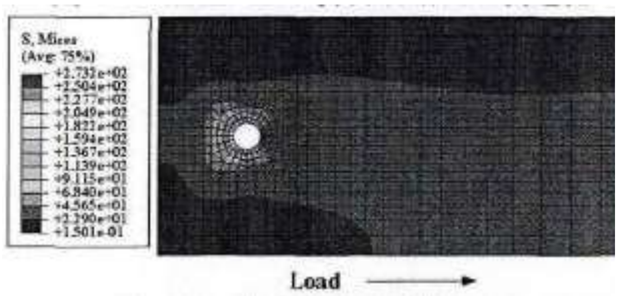

Figure 46 Stress diagram of open-hole steel plate (MPa)

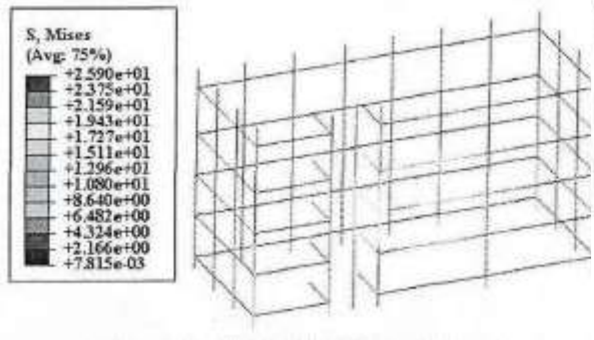

Figure 47 Stress diagram of ordinary steel bars (MPa)

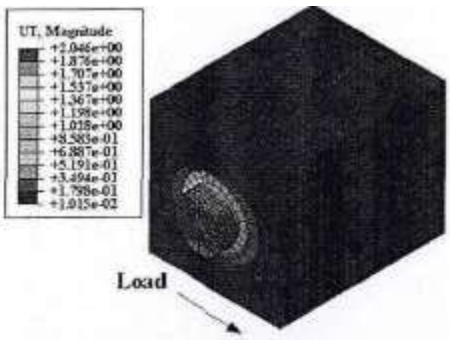

Figure 48 Concrete Deformation Diagram

ISSN 2055-6578(Print), ISSN 2055-6586(online)

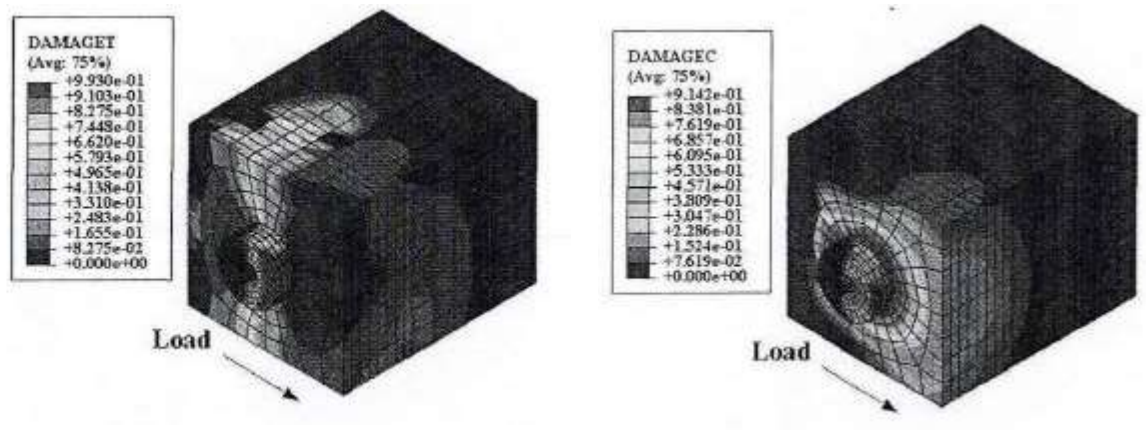

a) Distribution of the damage field near the concrete bar   b) Distribution of the pressure damage field

Figure 48 shows the damage distribution of concrete near concrete dowel.

From the distribution of the damage field of the tensile damage field, the tensile damage field is located on the side of the concrete dowel away from the loading direction and its surrounding area, while in the loading side the tensile damage is almost zero.

And the further away from the area of the shear bond, the smaller the tensile damage.

Figure b) is the cloud map of the pressure damage field. It can be seen that the pressure damage field is distributed on one side and the surrounding area of the concrete dowel loading direction.

The compression damage of the concrete is rapidly reduced away from the loading direction, and the distance from the shear bond is far. Concrete damage is almost zero; these are in line with the actual stress situation.

CONCLUSION

This paper discusses in detail the ABAQUS nonlinear finite element simulation method of embedded PBL shear bond and the verification of the calculation results.

The main research results are as follows:

1) The modeling process of ABAQUS simulation embedded PBL shear connector test is described in detail, and the precautions and related parameter settings in the modeling process are described in detail. The difficulty and focus of this type of component simulation is the fracture and failure of the concrete dowel. The accuracy of concrete material simulation directly determines the convergence and reliability of the model, and the boundary conditions and contact treatment is also the connector to the simulation. This modeling analysis can provide a reference for the modeling of homogeneous finite element analysis.

2) Comparing the results of the static general analysis with the test results, it can be seen that the load-slip curve of the finite element analysis agrees well with the experimental results, and there is a phenomenon of insufficient stiffness in the initial stage of the

ISSN 2055-6578(Print), ISSN 2055-6586(online)

calculation curve, which may not be simulated with the theoretical calculation model. In the initial stage, the bond effect of the steel plate is related to the concrete; the load-slip curve reflects the stiffness of the concrete dowel obtained by the finite element model when the slip amount is about 0.5 mm. According to the degradation map, the concrete dowel is almost cut off at this time, and the structure has entered the next stage of work; the damage patterns obtained by the finite element model are extracted separately and compared with the experimental phenomena, the two phenomena are mostly consistent, and the finite element analysis shows that the slip When the displacement is 1 mm, the through-reinforcing steel of A45-16-2S has already yielded full-section, and the stage of yielding of steel is longer, indicating that the working stage of the structure has been developed from concrete dowel and through-strand reinforcement to interface friction. The occlusion effect is used to bear the load.

3) The calculated load-slip curve is consistent with the experimental results and the concrete damage field distribution is consistent with the actual force, indicating that the concrete is damaged due to macroscopic The resulting structural stiffness degradation and the distribution and stress distribution of the damage field on the mesoscopic are reasonable. These conclusions further verify the correctness and reliability of the energy equivalent principle method from macroscopic and mesoscopic.

Acknowledgment

The research reported in the paper is part of the Project 51378427 supported by National zatural Science Foundation of China. Authors also would like to express sincere thanks to people who helped me to finish this paper, thanks for my entire classmate.

Author Contributions

All authors contributed to conceive the paper, analysis the date, mapping and Plotting.

Competing interests

The authors declare no competing of interest

Publisher's Note

Springer Nature remains neutral with regard to jurisdictional claims in published maps and institutional affiliations.

REFERENCES

[1] Hanswille G., Composite bridges in Germany-State of the Art [C]. Proceedings of 7^{th} German Japanese Bridge Symposium, Osaka, 2007.
[2] Nakamura S., Momiyama Y., Hosaka T., Homma K. New technologies of steel/concrete composite bridges Journal of Constructional Steel Research, 2002, 58(1): 99-130.
[3] ZELLNER W. Recent design of composite bridges and a new type of shear connector[A]. Proceedings of ASCE/LABSE Engineering Foundation Conference-Composite Construction in Steel and Concrete[C]. Henniker: New Hampshire, 1987. 240-252.

[4] Roberts W: S., HeyWood R. J.. Development and testing of a new shear connector for steel concrete composite bridges[J]. Fourth international bridge engineering conference,1995: 137-145.
[5] Oguejiofor E. C., Hosain M. U.. A parametric study of perfobond rib shear connectors. Can J Civil Eng, 1994;21:614-625.
[6] Oguejiofor E. C., Perfobond rib shear connectors for composite beams[M]. University of Saskatchewan, 1994.
[7] Valente I., Cruz P. J. S.. Experimental studies on shear connection between steel and lightweight concrete[J]. International conference on bridge maintenance, safety and management, 2, Kyoto, 2004
[8] Valente I., Cruz P. J. S.. Experimental analysis of Perfobond shear connection between steel and lightweight concrete[J]. Journal of constructional steel research, 2004,60:465-479.
[9] Valente I., Cruz P. J. S.. Design and experimental analysis of a new shear connector for steel and concrete composite structures[J]. International association for bridge maintenance and safety, 2004.
[10] Kim Hyeong-Yeol, Jeong Youn-Ju. Experimental investigation on behavior of steel-concrete composite bridge decks with perfobond ribs[J]. Journal of Constructional Steel Research, 2006, 62:463-471.
[11] Jeong Youn-Ju, Koo Hyun-Bon. Longitudinal shear resistance of steel-concrete composite slabs with penfobond shears connectors. Journal of Constructional Steel Research, 2009,65: 81-88.
[12] Ahn J.-H., Kim S.-H., Jeong Y-J.. Shear behavior of perfobond rib shear connector under static and cyclic loadings[J]. Magazine of concrete research, 2007,60(5):347-357.
[13] Ahn J. H., Kim S. H., Jeong Y. J.. Shear behaviour of perfobond rib shear connector under static and cyclic loadings[J]. Magazine of concrete research,2008,60(50): 347-357.
[14] Ahn Jin-Hee, Lee Chan-Goo, Won Jeong-Hun, Kim Sang-Hyo. Shear resistance of the perfobond-rib shear connector depending on concrete strength and rib arrangement[J]. Journal of Constructional Steel Research, 2010,66: 1295-1307.
[15] Vianna J.da.C., Costa-Neves L.F., Vellasco P.C.G. da S., Andrade S.A.L. de. Experimental assessment of Perfobond andT-perfobond shear connectors' structural response[J]. Journal of Constructional Steel Research, 2009,65: 408-421.
[16] Candido-Martins J.P.S, Costa-Neves L.F., Vellasco P.C.G. da S.. Experimental evaluation of the structural response of perfobond shear connectors[J]. Engineering structures, 2010,32: 1976-1985.
[17] Kim Sung-Hoon, Choi Jun-Hyeok. Experimental study on shear connection in unfilled composite steel grid bridge deck[J]. Journal of Constructional Steel Research, 2010,11(66):1339?1344.
[18] Oguejiofor E.C., Hosain M.U.. Numerical analysis of push-out specimens with perfobond rib connectors[J]. Computers & Structures,1997,62(4):617-624.
[19] Nguyen H. T., Kim S. E. Finite element modeling of push-out tests for Large stud shear connectors[J]. Journal of Constructional Steel Research,2009,65:1909-1920.
[20] Kim S. E., Nguyen H. T. Finite element modeling and analysis of a hybrid steel-PSC beam connection[J]. Engineering Structures,2010.
[21] Lubliner J, Oliver J, Oller S, et al. A Plastic-dam-age model for concrete[J].International Journal of Solids and Structures,1989,25(3):299-326.
[22] Lee J,Fenves G L.Plastic-damage model for cyclic loading of concrete structures[J].Journal of Engineering Mechanics, 1998,124(8):892-900.

ISSN 2055-6578(Print), ISSN 2055-6586(online)

[23] ABAQUS. Theory Manual Version 6.7. H.K.S.,2007.
[24] ABAQUS analysis user's manual v6.10[M].ABAQUS Inc,2010.
[25] Birtel V, Mark P. Parameterised finite element modeling of RC beam shear failure [C]. Proceedings of the 19th, Annual International ABAQUS Users' Conference. Boston, USA, 2006: 95-108.
[26] Mander J B,Priestley M J N,Park R.Theoretical stress-strain model for confined concrete[J].Journal of Structural Engineering,1988,114(8):1804-1826.
[27] Riks E. The application of Newton's method to the problem of elastic stability[J]. J. Appl. Mech., 1972,39: 1060-1066.
[28] BELYTSCHKO T, BLACK T. Elastic crack growth in finite elements with minimal remeshing [J]. Int J Numer Methods Eng, 1999, 45(5): 601-620.
[29] NAGASHIMA T, OMOTOY, TANI S. Stress intensity factor analysis of interface cracks using XFEM [J]. Int J Numer Methods Eng, 2003，56(8):1151-1173.
[30] STOLARSKA M, CHOPP D, MOES N, et al. Modelling crack growth by level sets in the extended finite element method [J]. Int J Numer Methods Eng, 2001，51(8): 943-960.
[31] DOLBOW J, MOES N, BELYTSCHKO T. An extended finite element method for modeling crack growth with frictional contact[J]. Comput Methods Appl Mech & Eng, 2001，190(51-52): 6825-6846.
[32] RETHORE J, GRAVOUIL A，COMBESCUREA. An energy-conserving scheme for dynamic crack growth using the extended finite element method [J]. Int J Numer Methods Eng, 2005，63(5): 631-659.
[33] Carmona J R, Ruiz G, del Viso J R. Mixed-mode crack propagation through reinforced concrete [J]. Engineering Fracture Mechanics, 2007, 74(17): 2788-2809.
[34] Raju I S. Calculation of strain-energy release rates with higher order and singular finite elements [J]. Engineering Fracture and Mechanics, 1987,28(3):251-274.
[35] Miravete A, Jimenez M A. Application of the finite element method to prediction onset of delamination growth [J]. Applied Mechanics Reviews, 2002, 55(2): 89-105.
[36] Carmona J R, Ruiz G, del Viso J R. Mixed-mode crack propagation through reinforced concrete [J]. Engineering Fracture Mechanics, 2007, 74(17): 2788-2809.

ISSN 2055-6578(Print), ISSN 2055-6586(online)